Dynamic Flexural Modulus and Low-Velocity Impact Response of Supercomposite™ Laminates with Vertical Z-Axis Milled Carbon Fiber Reinforcement

Suman Babu Ukyam[1], Raju P. Mantena[1], Damian L. Stoddard[1], Arunachalam M. Rajendran[1], Robert D. Moser[2]

[1]Department of Mechanical Engineering, University of Mississippi, Mississippi, USA
[2]Materials—US Army ERDC GSL, Vicksburg, Mississippi, USA
Email: sukyam@go.olemiss.edu, meprm@olemiss.edu, dlstodda@olemiss.edu, raj@olemiss.edu, Robert.D.Moser@usace.army.mil

Abstract

In work reported here, the dynamic properties and low-velocity impact response of woven carbon/epoxy laminates incorporating a novel 3D interlaminar reinforcement concept with dense layers of Z-axis oriented milled carbon fiber Supercomposite™ prepregs, are presented. Impulse-frequency response vibration technique is used for non-destructive evaluation of the dynamic flexural modulus (stiffness) and loss factor (intrinsic damping) of woven carbon/epoxy control and Supercomposite™ laminates. Low-velocity punch-shear tests were performed on control and Supercomposite™ laminates according to ASTM D3763 Standard using a drop-weight impact test system. Control panels had all layers of 3K plain woven carbon/epoxy prepregs, with a dense interlaminar reinforcement of milled carbon fibers in Z-direction used in designing the Supercomposite™ laminate—both having same areal density. Impulse-frequency response vibration experiments show that with a 50% replacement of woven carbon fabric in control panel with milled carbon fibers in Z direction dynamic flexural modulus reduced 25% - 30% (loss in stiffness) and damping increased by about the same 25% - 30%. Low-velocity punch-shear tests demonstrated about 25% reduction in energy absorption for Supercomposite™ laminates with the replacement of 50% woven carbon fabric in control panel.

Keywords

Supercomposite™, Damping Ratio, Dynamic Flexural Modulus, Milled Carbon

Fibers, Low-Velocity Punch-Shear

1. Introduction

Composite materials with unidirectional fibers or woven fabrics exhibit better in-plane strength and stiffness properties compared to those of metals and ceramics. However, usage of 2D composite laminates in aircraft and automobile applications has limitation due to low impact damage resistance and low through thickness mechanical properties when compared to conventional materials like aluminum alloys and steel. Absence of third direction reinforcement is attributed to the lower delamination resistance and out-of-plane properties. To improve interlaminar properties of 2D laminates, 3-dimensional textile preforms are being developed by using different manufacturing techniques like weaving, knitting, braiding, and stitching. Also, the undulations or crimps in the yarns may reduce mechanical properties such as tension or compression strengths. However, 3D reinforced composite materials are specially designed for bearing high stress in the third direction, impact, crash, energy absorption and multiaxial fatigue to overcome the disadvantages of standard laminated composite materials.

Hosur *et al*. [1] reported the critical results on stitched and unstitched woven carbon/epoxy laminates subjected to high strain-rate compression loading in a modified Split Hopkinson pressure bar. A 3-cord Kevlar thread was used for stitching dry fabric preforms in a lockstitch pattern with a stitch pitch of 6 mm. In both stitched and unstitched plain and satin weave samples, higher peak stress, higher modulus and low strain at peak stress were observed during dynamic loading when compared to static loading condition. The peak stress and modulus increased with increasing strain-rate for both unstitched plain and satin weave samples. Unstitched satin and plain weave laminates exhibited higher peak stress and modulus than stitched satin and plain weave laminates for both in-plane loading directions. Hosur *et al*. [2] also reported the response of stitched S2-Glass/SC-15 Epoxy composites under low-velocity impact and ballistic impact loading. Results indicated stitching considerably enhanced the damage resistance of the laminates by restricting the size of damage and improving ballistic limits. Baucom *et al*. [3] reported the damage accumulation in two-dimensional (2D) and three-dimensional (3D) woven glass-fiber-reinforced composite panels under repeated transverse drop-weight impact loading conditions. The fabric preform of the 2D composite was a 2D plain-woven laminate with four layers of S-2 Glass roving. The fabric preform of the 3D composite was a 3D orthogonal weave with approximately the same areal density as the 2D laminate. The 3D composites had the greatest resistance to penetration and dissipated more total energy than the 2D laminate systems. This damage tolerance is due to unique energy absorption mechanisms, which involve the crimped portion of Z-tows in

the 3D composites.

Grogan *et al.* [4] reported the ballistic resistance of sandwich composite structures for vehicle armor panel applications. The core material of each sandwich structure is a layer of tiled alumina ceramic, combined with a layer of 2D/3D S-2 glass-based woven composite laminate, sandwiched between 2D plain weave composite skins. The 2D composite backing consists of a plain-woven fiberglass, with fiber orientation predominantly in the direction of plane of the weave. The 3D contains similar in-plane fiber preform structure, with the inclusion of an integral through thickness fiber, creating a 3D structure. Armor panels with 3D woven backing controlled delaminated and fewer complete penetrations indicating a higher ballistic efficiency than the 2D baseline panels. Muñoz *et al.* [5] reported the damage caused on a 3D woven hybrid composite subjected to low-velocity impacts. 3D composite material was manufactured by vacuum infusion of an epoxy vinyl ester resin in 3D orthogonal woven preform. 3D orthogonal preform was made of several plies of woven Carbon and S2/glass fiber fabrics with Dyneema fiber as Z-yarn binder. 3D woven hybrid composite showed a better performance due to the confining effect of Z-yarns, which spread damage across the whole specimen. Hart *et al.* [6] studied the post-impact mechanical response of 2D and 3D woven glass/epoxy composite plates and beams of equivalent areal density. Composites with 3D woven reinforcement were fabricated from a single layer S2-glass orthogonal weave fabric consisting of 3 warp and 4 weft layers held by a through thickness penetrating Z-tow travelling in the warp direction. Composites with 2D woven reinforcement were made from 5 layers plain woven S2-glass fabric arranged in a $[0]_5$ configuration, yielding the same fiber areal density as the 3D woven composites. When 3D and 2D composites were subjected to low velocity impacts, delamination length and opening of 3D woven composites were less than 2D composites impact at the same energy level. 3D woven composites retained greater post-impact mechanical performance because of the through-thickness Z-tow.

Zhang *et al.* [7] investigated the low-velocity impact response of fabric composite laminates. Results showed that composite laminate of single-ply 3D orthogonal woven fabric exhibits better energy absorbing capacity and impact damage resistance compared to those of unidirectional and 2D plain woven fabric. Wang *et al.* [8] reported the low velocity impact properties of 3D woven hybrid composites. 3D woven composites showed higher ductile indices, lower peak load and higher specific energy absorption in both warp and weft directions than that of the intra-ply hybrid composite. Berk *et al.* [9] reported the experimental data on low velocity impact behavior of S2 glass/epoxy and aramid/epoxy composite plates. LS-DYNA was used to perform numerical simulations, experimental and numerical results were found to be in good agreement. Brahmananda Pramanik and Raju Mantena [10] reported the punch-shear response of nanoparticle reinforced vinyl ester plates, laminated face sheets and sandwich composites using Dynatup 8250 according to the ASTM D3763 standard. Results show more than

10% improvement in impact energy absorption with addition of 2.5 wt pct. graphite platelets to pure vinyl ester. EcoCore° sandwiched in between E-glass/vinyl ester face sheets showed approximately 85% more energy absorption than with Tycor°, Balsa wood and PVC foam cores.

Shafi *et al.* [11] studied the vibration damping characteristics of nanocomposites and uni-directional carbon fiber reinforced polymer composites (CFRP) containing carbon nanotubes (CNTs) using free and forced vibration tests. Damping ratio of CFRP-CNT hybrid composites increased with increasing CNT content in both free and forced vibration tests. Esma Avil *et al.* [12] investigated the contribution of the non-functionalized multi-walled carbon nanotubes on the vibration damping behavior of unidirectional and bidirectional continuous carbon fiber reinforced epoxy matrix composites. There was no additional contribution of CNTs to the flexural strength and modulus values, however, it was justified this could be due to the lower efficiency of the resin infusion process leading to insufficient impregnation of the CF layers with high viscosity CNT containing resin. Contribution of CNTs was significant in case of vibration damping.

In work reported here, the dynamic properties and energy absorption characteristics of woven carbon/epoxy laminates incorporating a different 3D interlaminar reinforcement concept with dense layers of Z-axis oriented milled carbon fiber Supercomposite™ prepregs, are evaluated. Control laminate had all layers of 3K plain woven carbon/epoxy prepregs with a dense interlaminar reinforcement of milled carbon fibers in Z-direction used for forming Supercomposite™ laminate—both having same areal density. Impulse-frequency response vibration technique is used for the non-destructive evaluation of dynamic flexural modulus (stiffness) and loss factor (intrinsic damping) of carbon/epoxy control and Supercomposite™ laminates. Suarez *et al.* [13], Gibson [14], and Mantena *et al* [15] [16] [17] [18] [19] have performed several studies for characterizing composite materials with this vibration based non-destructive evaluation technique. Dynamic flexural modulus and loss factor computed from the frequency response spectrum and closed-form methods are presented. Low velocity punch-shear tests were performed on control and Supercomposite™ plate specimens at 4.4 m/s according to ASTM D3763 Standard using a drop-weight impact test system. From the low-velocity punch-shear experiments, specific energy absorption was calculated using the force, energy and deflection plots.
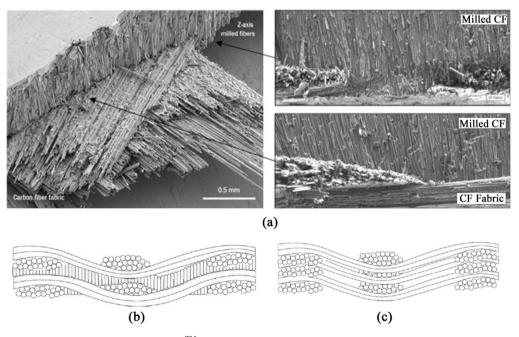
2. Materials and Test Specimens

In both control and Supercomposite™ prepregs, T300 3K plain weave carbon fabrics are used as fiber material. Areal weight of the carbon fabric is 205 gsm. 3K plain weave is a 1×1 weave with each warp strand floating over 1 fill strand then under 1 fill strand. A control ply is a T300 3K plain-weave carbon fabric impregnated with 45% of 250° F cure epoxy (Newport NB 301) resin (Figure 1(c)). Areal weight of control ply is 351 gsm.
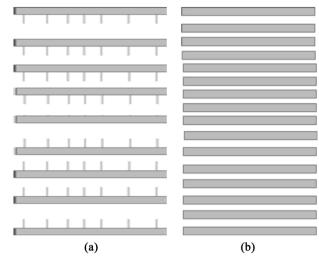
Supercomposite™ ply, a 3D prepreg with dense interlaminar reinforcement, is

formed by coating T300 3K plain-weave carbon fabric with Z-axis oriented milled carbon fibers at Boston Materials, LLC and impregnated with a 45% of 250˚ F cure epoxy (Newport NB 301) resin. Z-axis fibers are milled PX 30 - 150 μm type. Areal weight of Supercomposite™ ply is 667 gsm. These Z-axis milled fibers mechanically pin the layers of a laminated composite together as shown in Figure 1(a) and Figure 1(b), effectively increasing the interlaminar fracture toughness. This patented interlaminar toughening mechanism distributes multi-axial loads throughout the entire composite enabling the production of impact resistant and durable components designed for high-stress and high-temperature applications. Boston Materials, LLC supplies the Carbon Supercomposite™ as prepregs that are compatible with all automated tape laying and roll wrapping manufacturing methods. Under quasi-static loading conditions, these Z-axis milled fiber reinforcements are reported to have increased the toughness by about 300%, strength by 35% and Z-axis thermal conductivity by 300%, without any detriment to stiffness.

Both control and Supercomposite™ laminates of approximate equal thickness and areal weight density are designed and fabricated using control plies and Supercomposite™ plies. In the Supercomposite™ laminate, 8 Supercomposite™ plies and 1 control ply are stacked together 0˚/90˚ orientation to be symmetric by placing the control ply at the center location. To ensure mid-plane symmetry, the Z-axis milled fibers on top four Supercomposite™ plies and bottom four Supercomposite™ plies are oriented towards the control ply located at middle surface, as in Figure 2(a). In the control laminate, 16 control plies are stacked together at 0˚/90˚ orientation to be symmetric with respect to the middle surface

Figure 1. ((a), (b)) Supercomposite™ prepregs, and (c) Woven carbon/epoxy plies (courtesy: Boston Materials, LLC). (a) Z-axis milled fibers provide through-thickness & interlaminar reinforcement; (b) 2 in-plane Supercomposite™ prepregs; (c) 3 in-plane woven carbon/epoxy plies.

Figure 2. (a) Supercomposite^{TM} laminate, with 1 control ply of 3K plain weave carbon ply at center and eight Supercomposite^{TM} plies, and (b) Control laminate with 16 plies of 3K plain woven carbon/epoxy prepregs.

as in **Figure 2(b)**. Both control and Supercomposite^{TM} laminates are cured in an autoclave at 90 Psi for 3 hours. Temperature inside the autoclave is ramped linearly from room temperature up to 250˚ F in first 100 minutes, maintained at 250˚ F for next 50 minutes and ramped down to room temperature in the remaining time.

2.1. Impulse-Frequency Response Vibration Test Specimens

Rectangular specimens of 254 mm length by 19.05 mm width were cut from control and Supercomposite^{TM} laminates for the impulse-frequency response beam vibration tests as shown in **Figure 3(a)**. Specimens are fixed in a vise with a free length of 203.2 mm. Average thickness of control and Supercomposite^{TM} laminates is 3.95 mm. Cross-sectional view of Supercomposite^{TM} with Z-axis milled carbon fibers and control laminates captured using a KEYENCE digital microscope are shown in **Figure 3(b)** and **Figure 3(c)** respectively. Details of control and Supercomposite^{TM} laminates are listed in **Table 1**. Control specimens are represented by CBE and Supercomposite^{TM} laminates are represented by CZE.

2.2. Low Velocity Punch Shear Test Specimens

Square specimens of 101.6×101.6 mm were cut from control and Supercomposite^{TM} laminates for the low-velocity punch-shear tests. Details of control and Supercomposite^{TM} plate specimens used for experiments are listed in **Table 2**.

3. Experimental Procedure and Results
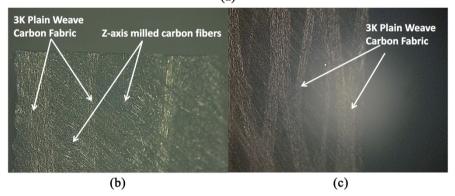
3.1. Impulse-Frequency Response Vibration Test

Specimens are clamped at one end in a fixed-free configuration and tapped with a Modally Tuned® impulse hammer (PCB 086C01) with force sensor. Vibration

Table 1. Control (CBE) and Supercomposite™ (CZE) specimens for vibration tests.

Specimen name	Cantilever length m	Cross section area m²	Area moment of inertia m⁴
CBE1	0.203	8.38E−05	1.19E−10
CBE2	0.203	8.18E−05	1.13E−10
CBE3	0.203	8.35E−05	1.17E−10
CZE1	0.203	7.51E−05	8.88E−11
CZE2	0.203	7.96E−05	1.04E−10
CZE3	0.203	7.29E−05	9.55E−11

Figure 3. (a) Control specimens (CBE1, CBE2 & CBE3) and Supercomposite™ specimens (CZE1, CZE2 & CZE3) for impulse-frequency response vibration test; (b) Cross section of Supercomposite™ laminate with Z-axis milled carbon fibers; (c) Cross section of woven carbon/epoxy control laminate.

Table 2. Control (CBE) and Supercomposite™ (CZE) specimens for low-velocity punch-shear tests.

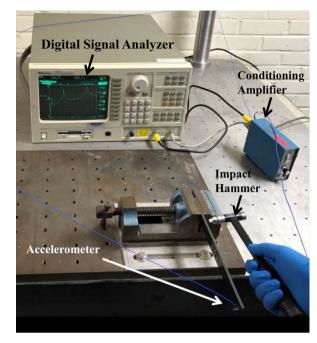| Specimen name	Volume density Kg/m³	Areal density Kg/m²	Thickness mm
CBE1	1414.04	5.66	4.00
CBE2	1433.12	5.49	3.83
CBE3	1455.12	5.55	3.82
CZE1	1404.40	5.66	4.03
CZE2	1436.05	5.53	3.85
CZE3	1457.53	5.68	3.90

Figure 4. Experimental setup with cantilever beam specimen in impulse-frequency response vibration test.

response is analyzed using HP Dynamic Signal Analyzer (35665A) through an accelerometer attached at the free end of the beam specimen (**Figure 4**). A Force-Exponential window is used with first, second and third resonant frequencies displayed. First resonant peak is curve fitted and closed-form solutions used for obtaining the dynamic flexural modulus. Damping ratio (ζ) corresponding to first natural frequency is obtained from the spectrum analyzer's built-in Nyquist plot analysis.

Under dynamic load conditions, Young's modulus for a viscoelastic material can be written in complex terms as [13] [14]:

$$E^* = E' + iE'' \tag{1}$$

Dynamic modulus (E') represents the elastic (real part) component of the complex modulus. This is the part of the modulus that is proportional to the stored energy that is recovered instantaneously. The loss modulus (E'') represents the part of the modulus that is dissipative and unrecovered. The loss factor implies the proportion of energy dissipated by the structure. Loss factor is given by

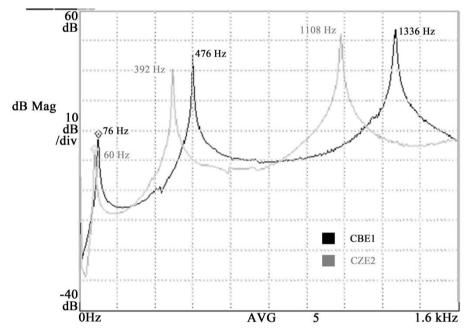$$\eta = \frac{E''}{E'} = 2\zeta \tag{2}$$

Dynamic flexural modulus is evaluated as [13] [14]

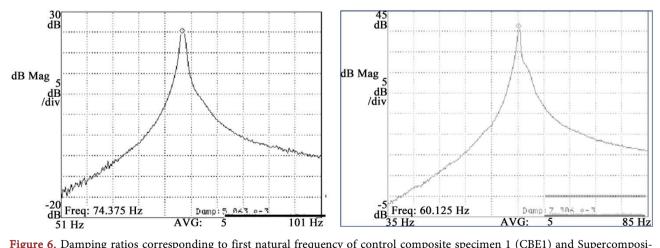$$E' = \frac{4\pi^2 f_1^2 L^4 \rho A}{\left(\lambda_1 L\right)^4 I} \tag{3}$$

where L is the cantilever free length, f_1 is first resonant frequency, ρ is the density, A is the cross sectional area, I is the area moment of Inertia and λ_1 is the Eigen value of the Ist mode. For 1st mode, $\lambda_1 L = 1.875$.

A plot showing first three natural frequencies of both control and Supercomposite™ cantilever beam specimens is shown in **Figure 5**. First three natural frequencies of control composites and Supercomposite™ cantilever beam specimens are shown in **Figure 5**. Damping ratios corresponding to first natural frequency were obtained experimentally by zooming near the first natural frequency with a shorter span for both control and Supercomposite™ as shown in **Figure 6**.

Experimental results from impulse-frequency response vibration tests are listed in **Table 3**. Dynamic flexural modulus is calculated using Equation (3). Resonant frequency of control composite cantilever beam specimens is around 74 Hz. Resonant frequency of Supercomposite™ cantilever beam specimens is
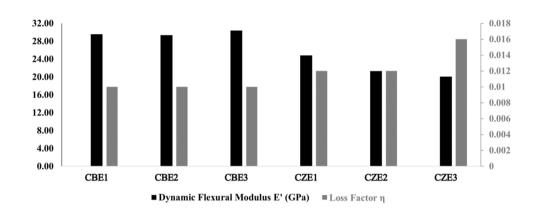

Figure 5. First, second, and third natural frequencies of control composite specimen 1 (CBE1) and Supercomposite™ Specimen 2 (CZE2).
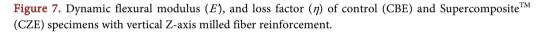

Figure 6. Damping ratios corresponding to first natural frequency of control composite specimen 1 (CBE1) and Supercomposite™ Specimen 2 (CZE2).

Table 3. Resonant frequency, dynamic flexural modulus and loss factor of control (CBE) and Supercomposite™ (CZE) laminates.

Specimen name	Resonant frequency Hz	Damping ratio Ratio	Loss factor η Factor	Dynamic Flexural Modulus E' GPa	Loss modulus E'' GPa
CBE1	74.18	0.005	0.010	29.54	0.30
CBE2	72.78	0.005	0.010	29.34	0.29
CBE3	74.75	0.005	0.010	30.34	0.30
CZE1	61.78	0.006	0.012	24.82	0.30
CZE2	61.70	0.006	0.012	21.28	0.26
CZE3	60.38	0.008	0.016	20.05	0.32

Figure 7. Dynamic flexural modulus (E'), and loss factor (η) of control (CBE) and Supercomposite™ (CZE) specimens with vertical Z-axis milled fiber reinforcement.

around 61 Hz. A drop in resonant frequency is observed in case of Supercomposite™ laminate with almost 50% reduction in woven carbon fabric content.

Dynamic flexural modulus and loss factor for control and Supercomposite™ laminates are summarized in **Figure 7**. Experimental results show that by replacing about 50% woven carbon fabric in control panel with milled carbon fibers in Z-direction; dynamic flexural modulus reduced 25% - 30% (loss in stiffness) and damping increased by about the same 25% - 30%.

Under flexural vibration of a cantilever beam specimen, both tensile and compressive normal strains are induced respectively above and below the neutral surface, along with some shear strain. Higher normal strains occurring in plies away from neutral surface will cause a separation of vertical Z-axis milled fibers in the interlaminar Supercomposite™ prepregs, resulting in a reduction of dynamic flexural modulus. Shear strains, on the other hand, contribute to increase in damping (loss factor) through interfacial rubbing of the embedded vertical Z-axis milled fibers in Supercomposite™ prepregs. These two factors simultaneously resulted in a reduction of dynamic flexural modulus and increase in damping with the uniform layup of milled carbon fibers (through the thickness) employed in this research. Placing more layers of woven carbon/epoxy control

plies away from neutral surface would result in a less significant drop in dynamic flexural modulus along with enhanced damping.
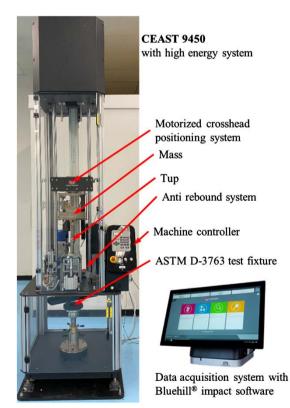
3.2. Low Velocity Punch Shear Test

Low-velocity punch shear experiments were performed on control and Super-composite™ laminates using a CEAST 9450 Drop Tower Impact Test System (Figure 8). Square plate specimens are impacted by a hemispherical-head plunger (19.05 mm diameter, 5.5 kg) with an additional mass of 25 kg. A fixed circular boundary condition with a 76.2 mm diameter hole on both top and bottom surfaces of the specimen was imposed during the impact test and clamped with a uniform pressure of 0.6 MPa. ASTM D3763 test method mandates the velocity slowdown at peak load to be below 20%. Impact energy was calculated to be at least three times the energy absorbed, so that there is no appreciable slowdown of the tup during the impact event.

Impact energy was assessed to be 302 J using trial specimens. The impact velocity was calculated based on conservation of energy principle,

$$\text{Impact energy} = \frac{1}{2}mv^2 = mgh \tag{4}$$

where m is the total mass of the falling weight, v is impact velocity, h is height of the impactor from the sample surface, and g is acceleration due to gravity. With a total mass of 30.5 kg, height and impact velocity are 1 m and 4.45 m/s, respectively.

Figure 8. CEAST 9450 drop weight impact system with pneumatic assist and data acquisition system dashboard—experimental setup for low-velocity punch-shear test.

The Bluehill® Impact software provides force, energy, velocity, and deflection histories over the time of impact. Force vs Time, Force vs Deflection, and Energy vs Deflection were obtained for each test. 1st order Butterworth—low pass filter with a cutoff frequency of 1360 Hz was used for filtering the data. Force vs Time, Force vs Deflection and Energy vs Deflection curves of control and Supercomposite™ plate specimens subjected to low-velocity punch-shear tests are plotted in Figures 9-11, respectively. A sample of Force vs Deflection and Energy vs Deflection of the control and Supercomposite™ plate specimens are plotted simultaneously in Figure 12.

In Figure 9, the contact force-time history is measured from the point of initial contact, and as the plunger traverses through the specimen. Energy absorption is calculated from integration of the Force-Deflection signal. Force-time histories provide a good indication of the progression of damage in the composites sample. The Force-time history is observed to be asymmetrical and the oscillations represent progressive impact damage as the plunger penetrates through the specimen.

P_i, the incipient damage and E_i, incipient energy points are the first significant deviations from the initial portion of the Force-time curve. E_i, corresponding to P_i can be obtained from Energy vs Deflection curve as in Figure 11 and Figure 12. Point of incipient damage indicates matrix microcracking, fiber damage or onset of delamination. From Figure 10, the initial slope (stiffness) of Force vs Deflection curve indicates that control plates have higher stiffness relative to Supercomposite™ plates during damage initiation process. Average stiffness of control panel and Supercomposite™ were 1541 N/mm and 1147 N/mm,
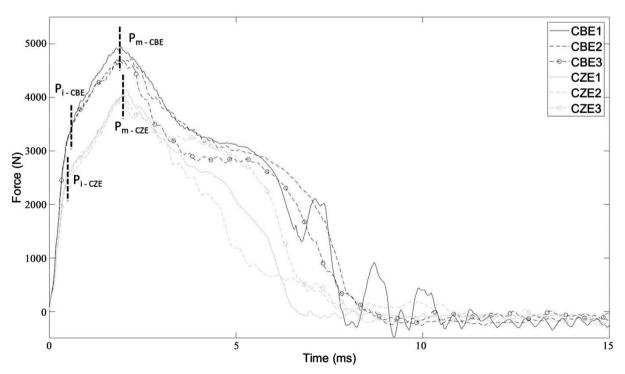

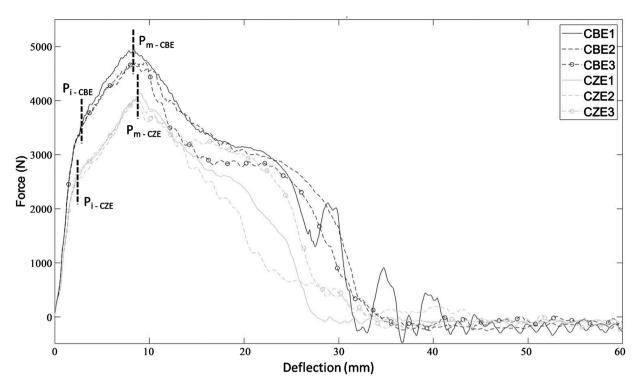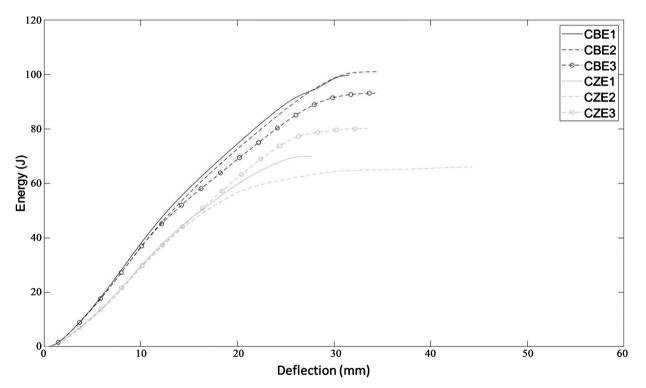**Figure 9.** Force vs Time response of control and Supercomposite™ specimens.

Figure 10. Force vs Deflection response of control and Supercomposite™ specimens.

Figure 11. Energy vs Deflection curves up to total load point P_t for control and Supercomposite™ specimens.

respectively. About 25% reduction in stiffness was observed in Supercomposite™ specimens comparable to the 25 percent drop in dynamic flexural modulus from Impulse-frequency response vibration experiments. After P_i, a substantial
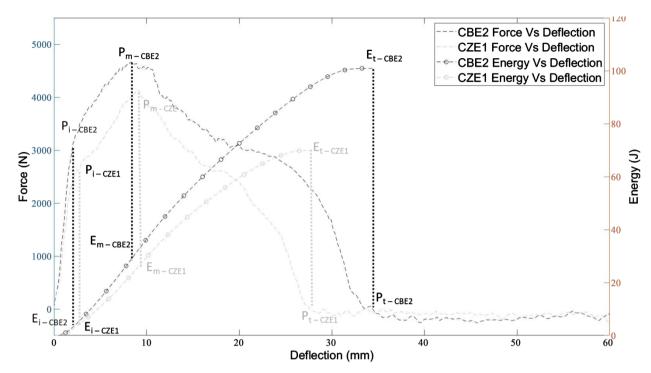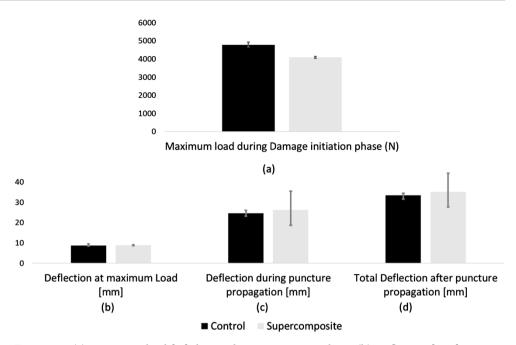
Figure 12. Force vs Deflection and Energy vs Deflection for a control (CBE2) and a Supercomposite™ (CZE1) specimen.

decrease in stiffness was observed for both control and Supercomposite™ plates up to a maximum load of P_m. The Force vs Deflection curves of both the control and Supercomposite™ plates are nearly parallel, resulting in a slight variation in stiffness.

Damage initiation phase is observed from the moment of impact to the point of maximum load, P_m. The point of maximum load (P_m) and energy (E_m) signifies the end of damage initiation phase or rebound. At the point of maximum load, puncture is initiated, and puncture propagation is followed by a rapid load reduction. When impacted at the same energy level of 302 J, maximum load, P_m in control specimens was higher than in Supercomposite™ specimens. Around 15% drop in maximum load was observed for Supercomposite™ specimens as shown in **Figure 13(a)**.

Puncture propagation takes place up to total load point, P_t. Total energy absorption E_t was calculated as the sum of energy absorbed for damage initiation and puncture propagation phases up to complete failure of the specimen. In **Figure 11**, Energy vs deflection curve is plotted up to total load point, P_t. Constant energy profile past the maximum load indicates that all the impact energy is absorbed by the specimen. Total energy absorbed by control and Supercomposite™ specimens up to total load point, P_t is shown in **Figure 11**. Total energy absorption was higher in control plate specimens when impacted at the same energy level (**Figure 14**). During puncture propagation phase, deflection in Supercomposite™ specimens was higher than the deflection in control specimens as in **Figure 13(c)** and **Figure 13(d)**.

Penetration mode of failure was observed for all the specimens and impacted

Figure 13. (a) Maximum load [N] during damage initiation phase, (b) Deflection [mm] at maximum load P_m, (c) Deflection [mm] during puncture propagation, and (d) Total deflection [mm] up to total load point P_t.
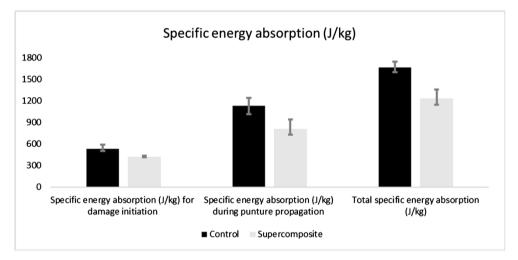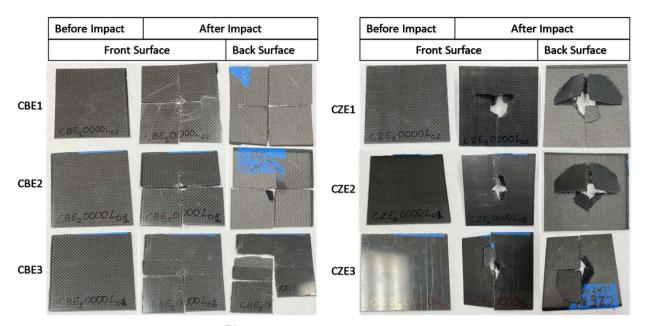

Figure 14. Specific energy absorption of control and Supercomposite^{TM} specimens.

energy was absorbed by the specimens as seen in the Energy vs Deflection curves. Fiber failure occurred enabling the impactor to penetrate through the material. Shear, delamination, and elastic flexure are the major mechanisms of energy absorption during the penetration. Penetration process is influenced by various factors including tow size, fiber sizing, fiber orientation, weave type, matrix type and interfacial mechanisms have influence on the penetration process.

Energy absorption during damage initiation phase and puncture propagation phase are normalized with respect to mass for comparing the specific energy absorption capacity of control and Supercomposite^{TM} plate specimens (**Figure 14**). Specific energy absorption (J/kg) of control specimens was higher than the

Figure 15. Control and Supercomposite™ square plates subjected to low-velocity punch-shear in a CEAST 9450 drop weight impact system.

Supercomposite™ specimens during damage initiation and puncture propagation phases. As observed, the total specific energy absorption was high for control specimens. About 50% replacement of woven carbon fabric in control panel with milled carbon fibers in Z-direction resulted in about 25% reduction of total specific energy absorption (J/kg).

Figure 15 shows both the control and Supercomposite™ square plate specimens that were subjected to low-velocity punch-shear in the CEAST 9450 drop weight impact test system. Visual inspection of control specimens illustrates diametric cracks with woven fiber breakage as the predominant damage mechanisms during puncture propagation. Supercomposite™ specimens, on the other hand, exhibited through shear failure during penetration with woven fiber breakage along with some interlaminar separation around the impact zone. The Z-axis aligned milled carbon fiber forest appears to be ineffectual in resisting impactor penetration in vertical Z-direction, therefore the lower specific energy absorption during puncture propagation phase (Figure 14).

4. Conclusions

Dynamic properties of woven carbon/epoxy laminates incorporating a novel 3D interlaminar reinforcement concept with dense layers of Z-axis oriented milled carbon fiber Supercomposite™ prepregs, have been analyzed using the impulse-frequency response vibration technique. About 50% replacement of woven carbon fabric in control panel with milled carbon fibers in Z-direction resulted in 25% - 30% reduction of dynamic flexural modulus (loss in stiffness) along with 25% - 30% increase in damping. In the work reported here, woven carbon/epoxy fabric content in control panel was replaced with 50% Supercomposite™ prepregs

for preserving the same areal density.

Impact load, deflection, and energy plots along with visual inspection of post damaged specimens illustrated the failure characteristics and punch shear response of composites reinforced with Z axis milled carbon fibers. If the composite laminate is designed for a containment vessel for e.g., occurrence of incipient crack damage on Force vs Deflection curve is used for calculating energy and time of damage initiation during the impact event. If the primary function of the composite laminate is to absorb a large amount of energy, values of energy at peak load and the total energy along with time taken to reach those values demonstrates the specimen's capacity to absorb and/or re-distribute the impact energy. About 50 percent replacement of woven carbon fabric in the control panel resulted in a reduction of around 25 percent in initial stiffness up to incipient load point (consistent with impulse-frequency response vibration test results) and total specific energy absorption, along with a 15 percent reduction in maximum load bearing capacity.

It may be noted, however, that further enhancements to dynamic stiffness, damping, interlaminar properties, initial slope (stiffness) in damage initiation, maximum load bearing capacity and total specific energy absorption may be achieved by adjusting both the location and quantity of Z-axis milled carbon fiber Supercomposite™ prepregs within the laminate.

Acknowledgements

Conflicts of Interest

The authors declare no conflicts of interest regarding the publication of this paper.

References

[1] Hosur, M.V., Adya, M., Vaidya, U.K., *et al.* (2003) Effect of Stitching and Weave Architecture on the High Strain Rate Compression Response of Affordable Woven Carbon/Epoxy Composites. *Composite Structures*, **59**, 507-523. https://doi.org/10.1016/S0263-8223(02)00247-7

[2] Hosur, M.V., Karim, M.R. and Jeelani, S. (2004) Studies on Stitched Woven S2 Glass/Epoxy Laminates under Low Velocity and Ballistic Impact Loading. *Journal of Reinforced Plastics and Composites*, **23**, 1313-1323. https://doi.org/10.1177/0731684404037048

[3] Baucom, J.N., Zikry, M.A. and Rajendran, A.M. (2006) Low-Velocity Impact Damage Accumulation in Woven S2-Glass Composite Systems. *Composites Science and Technology*, **66**, 1229-1238. https://doi.org/10.1016/j.compscitech.2005.11.005

[4] Grogan, J., Tekalur, S.A., Shukla, A., *et al.* (2007) Ballistic Resistance of 2D and 3D Woven Sandwich Composites. *Journal of Sandwich Structures & Materials*, **9**, 283-302. https://doi.org/10.1177/1099636207067133

[5]   Munoz, R., Seltzer, R., Sket, F., *et al.* (2012) Mechanical Characterization of 3D Woven Materials against Impact Loads. 15*th European Conference on Composite Materials*, Venice, Italy, 24-28 June 2012, 1-6.

[6]   Hart, K.R., Chia, P.X.L., Sheridan, L.E., *et al.* (2017) Comparison of Compression-after-Impact and Flexure-after-Impact Protocols for 2D and 3D Woven Fiber-Reinforced Composites. *Composites Part A*: *Applied Science and Manufacturing*, **101**, 471-479. https://doi.org/10.1016/j.compositesa.2017.07.005

[7]   Zhang, D.T., Sun, Y., Chen, L. and Pan, N. (2013) A Comparative Study on Low-Velocity Impact Response of Fabric Composite Laminates. *Materials and Design*, **50**, 750-756. https://doi.org/10.1016/j.matdes.2013.03.044

[8]   Wang, X., Hu, B., Feng, Y., Liang, F., Mo, J., Xiong, J. and Qiu, Y. (2008) Low Velocity Impact Properties of 3D Woven Basalt/Aramid Hybrid Composites. *Composites Science and Technology*, **68**, 444-450. https://doi.org/10.1016/j.compscitech.2007.06.016

[9]   Berk, B., Karakuzu, R., Icten, B.M., Arikan, V., Arman, Y., Atas, C. and Goren, A. (2016) An Experimental and Numerical Investigation on Low Velocity Impact Behavior of Composite Plates. *Journal of Composite Materials*, **50**, 3551-3559. https://doi.org/10.1177/0021998315622805

[10] Pramanik, B. and Mantena, P.R. (2009) Low Velocity Punch-Shear Response of Nanoclay and Graphite Platelet Reinforced Vinyl Ester Plates, Laminated Face Sheets and Sandwich Composites. *ASME* 2009 *International Mechanical Engineering Congress and Exposition*, Lake Buena Vista, Florida, USA, 13-19 November 2009, 223-224. https://doi.org/10.1115/IMECE2009-12180

[11] Khan, S.U., Li, C.Y., Siddiqui, N.A., *et al.* (2011) Vibration Damping Characteristics of Carbon Fiber-Reinforced Composites Containing Multi-Walled Carbon Nanotubes. *Composites Science and Technology*, **71**, 1486-1494. https://doi.org/10.1016/j.compscitech.2011.03.022

[12] Avil, E., Kadioglu, F. and Kaynak, C. (2020) Contribution of Carbon Nanotubes to Vibration Damping Behavior of Epoxy and Its Carbon Fiber Composites. *Journal of Reinforced Plastics and Composites*, **39**, 311-323. https://doi.org/10.1177/0731684420906609

[13] Suarez, S.A. and Gibson, R.F. (1987) Improved Impulse-Frequency Response Techniques for Measurement of Dynamic Mechanical Properties of Composite Materials. *Journal of Testing and Evaluation*, **15**, 114-121. https://doi.org/10.1520/JTE10991J

[14] Gibson, R.F. (2000) Modal Vibration Response Measurements for Characterization of Composite Materials and Structures. *Composites Science and Technology*, **60**, 2769-2780. https://doi.org/10.1016/S0266-3538(00)00092-0

[15] Mantena, P.R., Gibson, R.F. and Hwang, S.J. (1991) Optimal Constrained Viscoelastic Tape Lengths for Maximizing Damping in Laminated Composites. *AIAA Journal*, **29**, 1678-1685. https://doi.org/10.2514/3.10790

[16] Mantena, P.R. (1991) NDE Applications of Damping Measurements. *Proceedings of the* 11*th National Conference on Noise Control Engineering*, Tarrytown, NY, 14-16 July 1991, 361-368.

[17] Mantena, P.R., Vangipuram, R. and Barpanda, D. (1993) Quality Monitoring of Pultruded Glass-Epoxy Composites with Vibration Damping Measurements. *Dynamic Characterization of Advanced Materials ASME*, **16**, 51-57.

[18] Mantena, P.R., Vangipuram, R. and Vaughan, J.G. (1994) Dynamic Flexural Properties of Pultruded Glass/Graphite Hybrid Composites. 39*th International SAMPE*

Symposium, **39**, 174-182.

[19] Vangipuram, R., Mantena, P.R. and Hickling, R. (1994) Material Property Characterization of Pultruded Glass/Epoxy Composites Using Ultrasonic and Vibration Measurements. *NOISE-CON* 94, Fort Lauderdale, Florida, 1-4 May, 1994, 831-836.